Solar Energy Materials & Solar Cells 94 (2010) 366–375

Contents lists available at ScienceDirect

Solar Energy Materials & Solar Cells

journal homepage: www.elsevier.com/locate/solmat

Simultaneous determination of carrier lifetime and electron density-of-states in P3HT:PCBM organic solar cells under illumination by impedance spectroscopy

Germà Garcia-Belmonte [a,*], Pablo P. Boix [a], Juan Bisquert [a,*], Michele Sessolo [b], Henk J. Bolink [b]

[a] Photovoltaic and Optolectronic Devices Group, Departament de Física, Universitat Jaume I, ES-12071 Castelló, Spain
[b] Molecular Science Institute, Universitat de València, ES-46980 Paterna, Spain

ARTICLE INFO

Article history:
Received 24 July 2009
Received in revised form
14 October 2009
Accepted 15 October 2009
Available online 13 November 2009

Keywords:
Impedance spectroscopy
Lifetime
Organic solar cell
Bulk heterojunction

ABSTRACT

We report new insights into recombination kinetics in poly(3-hexylthiophene):methanofullerene (P3HT:PCBM) bulk heterojunction (BHJ) solar cells, based on simultaneous determination of the density of states (DOS), internal recombination resistance, and carrier lifetime, at different steady states, by impedance spectroscopy. A set of measurements at open circuit under illumination was performed aiming to better understand the limitations to the photovoltage, which in this class of solar cells remains far below the theoretical limit which is the difference between the LUMO level of PCBM and the HOMO of P3HT ($\sim$1.1 eV). Recombination kinetics follows a bimolecular law, being the recombination time (lifetime) inversely proportional to the density of photogenerated charges and the recombination coefficient $\gamma = 6 \times 10^{-13}$ cm^3 s^{-1}. We find that the open-circuit photovoltage is governed by the carrier ability of occupying the DOS, which results in Gaussian shape and spreads in energy $\sigma \approx 125$–140 meV. The energy position of the Gaussian DOS center (E_L=0.75–0.80 eV), which corresponds to half occupation of the electron DOS, approximates LUMO(PCBM)–HOMO(P3HT) difference. But the recombination rate is strongly enhanced at high illumination levels, what produces the photogenerated charge to remain in the tail of the DOS. Consequently, the electron and hole Fermi levels are unable to reach the center of the DOS, then substantially limiting the photovoltage. Detailed theoretical analysis of the lifetime dependence on photovoltage is provided.

1. Introduction

Bulk heterojunctions (BHJ) formed by an interpenetrating blend of an optically active polymer and electron accepting molecules constitute a very promising route towards cheap and versatile solar cells [1,2], as recently demonstrated in progress of automated roll-to-roll processing and solar-cell stability [3,4]. The photovoltaic performance of the combination of poly(3-hexylthiophene) (P3HT) and [6,6]-phenyl C_{61}-butyric acid methyl ester (PCBM) in organic blends has recently increased rapidly, approaching 6% energy-conversion efficiency [5], and 6.1% efficiency was achieved using poly[*N*-9"-hepta-decanyl-2,7-carbazole-alt-5,5-(4',7'-di-2-thienyl-2',1',3'-benzothiadiazole) (PCDTBT) and fullerene derivative [6,6]-phenyl C_{70}-butyric acid methyl ester ($PC_{70}BM$) blends [2]. Further improvements of BHJs based on rational design of materials and interfaces require characterization methods that provide elementary electronic parameters in the working conditions of the solar cell. In particular it is very important to ascertain (i) factors affecting open-circuit photovoltage V_{oc} [6,7], and closely related to this, (ii) the mechanism governing recombination kinetics of photogenerated charge.

Impedance Spectroscopy (IS) has provided enormous success for the determination of energetic and kinetic factors governing the operation of dye-sensitized solar cells (DSC) [8,9]. While IS measurement is quite straightforward, interpretation of the results requires an appropriate conceptual framework adapted to the specific features of a kind of devices. IS is a small perturbation method that resolves the capacitances and resistances in the system at a particular steady state. For solar-cell characterization, the most significant range of steady-state conditions is between open-circuit voltage (V_{oc}) and short circuit under illumination. Close to zero bias voltage, the operation of reasonably efficient solar cells (with a high collection efficiency [2]) is usually determined by charge generation. On another hand, in the maximum power point and close to V_{oc}, recombination kinetics plays a major role in the current density/potential (J–V)

* Corresponding authors. Tel.: +34 964 728040; fax: +34 964 729218.
(G. Garcia-Belmonte), Tel.: +34 964 728039; fax: +34 964 729218 (J. Bisquert).
E-mail addresses: garciag@uji.es (G. Garcia-Belmonte), bisquert@uji.es (J. Bisquert).

0927-0248/$ - see front matter © 2009 Elsevier B.V. All rights reserved.
doi:10.1016/j.solmat.2009.10.015

curve, and hence on the device efficiency [10]. Therefore a quantitative interpretation and modeling of the IS results in this bias region provides essential information on device characteristics.

In the case of DSCs, determination of electron lifetimes by IS at voltages close to V_{oc} has been validated with independent methods of measurement, such as open-circuit voltage decay [9,11,12]. In inorganic solar cells, it is possible to apply contactless methods to determine minority carrier lifetime [13], and IS results are in agreement with these methods too [14,15]. The convergence of different experimental methods provides great confidence on the significance of the results obtained by IS. We report in this paper for the first time the application of IS to determine simultaneously the charging characteristics (capacitance) and recombination kinetics of BHJ solar cells in working conditions, under illumination. The results show that energy disorder in the electron and hole conducting materials plays a major role to determine detailed features of carrier lifetime, and models appropriate to interpret the experimental results are derived below.

Several techniques have been applied to extract recombination time [16] (lifetimes) in BHJ devices, including modulated photo-induced absorption [17], transient absorption [18] photo-CELIV [19,20], double-injection currents [21], and time-of-flight methods [22]. However many of these methods do not operate in open-circuit conditions under continuous irradiation what makes it difficult to relate them to the cell operation. Recently, two papers have determined the capacitance and lifetime by small-amplitude perturbation of a steady state, using transient photovoltage [23] and impedance spectroscopy [24]. In these works, it was observed that when the Fermi level of electrons, E_{Fn}, increases, then (i) the lifetime decreases and (ii) the capacitance increases [23,24]. These results indicate that it is possible to separate in BHJs the carrier density and kinetic terms in the time constant for recombination, provided that the chemical capacitance [25], C_μ, can be measured, which provides access to the density-of-states (DOS) of the electron transporting phase [26,27]. However, in Ref. [23] capacitance and lifetime are measured in different conditions, and in Ref. [24] only the dark values have been estimated, and the capacitance was found to decrease at strong forward bias. In the present work, the capacitance and recombination resistance of a state-of-art P3HT:PCBM BHJ device, with 3.1% energy conversion efficiency, are simultaneously monitored under illumination as a function of V_{oc}.

These results allow us to address important questions concerning BHJ operation. First, in contrast to Ref. [23] we obtain that the lifetime is inversely proportional to steady-state carrier density, which indicates that recombination probability is proportional to both electron and hole concentration. In addition, based on thermodynamic principles, the open-circuit voltage is directly related to the separation between E_{Fn}, and the Fermi level of holes in the P3HT, E_{Fp}[28]

$$-qV_{oc} = E_{Fn} - E_{Fp} \tag{1}$$

being q the elementary charge. One upper limit to V_{oc} in this kind of devices is the difference of energies between the donor highest occupied molecular orbital, E_{HOMO}, and the acceptor lowest unoccupied molecular orbital, E_{LUMO}. Since at these energy levels the density of states is very high and no further split of Fermi levels is possible, we should obtain $V_{oc} \approx E_g/q$, where $E_g = E_{HOMO} - E_{LUMO}$, which can be interpreted as the effective (electrical) band gap of the blend. However, such limit is not reached in practice, instead a linear correlation between V_{oc} and the E_g/q is obtained, with an average shift of $\sim$0.3 V [29].

Since molecular orbitals in disordered media spread in energy, the shape of the DOS corresponding to electronic levels should play a significant role in establishing V_{oc} values. In fact $E_{Fn} - E_{Fp}$ difference must be governed both by the shape of the DOS around the *effective* E_{HOMO} and E_{LUMO} values, and by the extent of filling of available states which is established by the recombination rate. Therefore, we conclude in this paper that both issues, the V_{oc} origin and charge-carrier recombination are closely related: the DOS occupancy (carrier density) is limited by recombination losses at high ($\sim$1 sun) illumination levels, which in turn establishes the reachable V_{oc} value.

2. Experimental

Solar cells of structure ITO/PEDOT:PSS/P3HT:PCBM/LiF/Al were built following the procedure explained elsewhere [30]. The thickness of the P3HT:PCBM blend layers was approximately equal to 115 nm. The impedance measurements, both in the dark and under illumination up to simulated air mass 1.5 global (AM1.5 G) conditions, were carried out in an electrically shielded box, that was integrated in an inert atmosphere (<0.1 ppm O_2 and H_2O) glovebox. The impedance measurements were performed with an Autolab PGSTAT-30 equipped with a frequency analyzer module in the frequency range of $10^6 - 1$ Hz. Ac oscillating amplitude was as low as 20 mV (rms) to maintain the linearity of the response. In order to measure under zero-current conditions, a bias voltage was applied which equaled the open-circuit voltage obtained at each irradiation level. Temperature was controlled at the solar-cell location (22 ± 1 °C) using a Peltier cell, otherwise temperatures >40 °C were reached at 1 sun irradiation level. The solar cells exhibited photoresponse behavior when illuminated by a UV-filtered halogen lamp typical for these materials in the described device layout, namely: $V_{oc} \approx 0.60$ V, $I_{sc} \approx 10.2$ mA cm^{-2}, $FF \approx 52\%$, and efficiency $\eta \approx 3.1\%$ at 1 sun illumination.

3. Results and discussion

The impedance results at different illumination intensities are shown in Fig. 1. As mentioned before, the applied bias voltage compensates the effect of the photovoltage so that effectively the cell is measured at open-circuit conditions, i.e., photocurrent is cancelled by the recombination flow and j_{dc}=0. The spectra are characterized by a major *RC* arc plus additional minor features at high frequency. The high-frequency part of the spectra may contain information of transport and series resistance elements, as well as dielectric contributions [24], however these effects will not be further treated in this paper. The low-frequency arc is attributed to recombination in the photoactive blend [9] and the capacitance, resistance, and lifetime values, as a function of bias voltage, are shown in Fig. 2. The resistance of the arc is the differential recombination resistance R_{rec}, which is related to the recombination current density j_{rec} as

$$R_{rec} = \frac{1}{A}\left(\frac{dj_{rec}}{dV_{oc}}\right)^{-1} \tag{2}$$

with A being the device area [Fig. 2(b)].

3.1. Interpretation of the capacitance

The distribution of carriers as a function of bias voltage will be next inferred from the measured capacitance shown in Fig. 2(a). The capacitance results can be well understood using a model previously described for BHJ in dark conditions [24] that is very similar to that used for crystalline Si solar cells [15]. At open-circuit conditions macroscopic electrical field inside the active

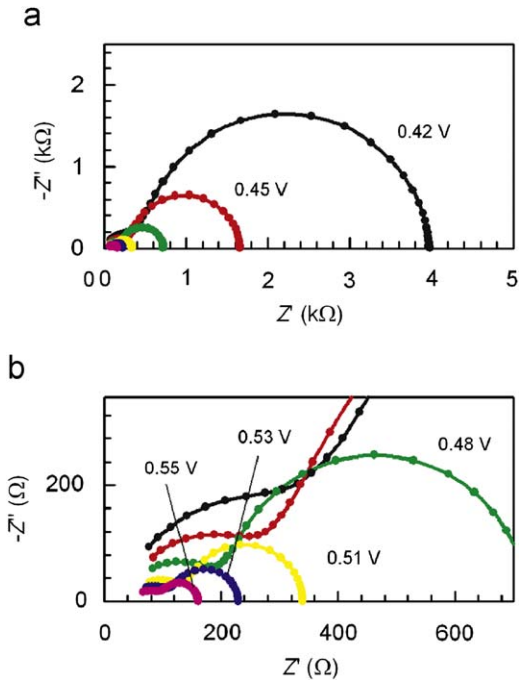

Fig. 1. Impedance spectra measured under different irradiation intensities (open-circuit conditions). V_{oc} is marked in each spectra. The low-frequency response is modeled by means of a parallel *RC* subcircuit. (a) Complete response (b) detail at high-illumination conditions.

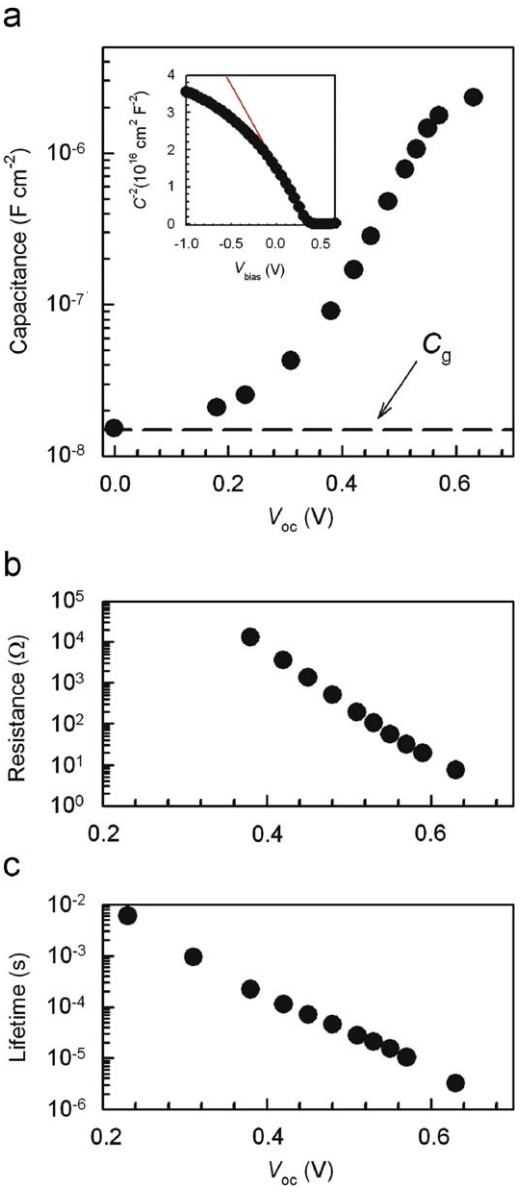

Fig. 2. (a) Capacitance values extracted from fits of the low-frequency arc of the impedance spectra in Fig. 1 as a function of V_{oc}. In the inset: Mott–Schottky curve (1 kHz) in the dark which exhibits a straight line yielding $N_A \approx 10^{15}\,\mathrm{cm}^{-3}$, assuming ε=3 for P3HT:PCBM. (b) Recombination resistance as a function of V_{oc} resulting from the analysis of low-frequency impedance under various illumination levels (0.01-1 sun), following $R_{rec} \propto \exp(-0.76V_{oc}/kT)$ (c) Recombination time (effective lifetime) as a function of V_{oc} calculated from the *RC* time constant.

layer must be negligible, except at the metal contact where a Schottky barrier may be formed. In fact it has been shown in P3HT:PCBM that band bending with a corresponding depletion zone occurs at the cathode, the P3HT-Aluminum contact [31]. This is because P3HT is a conjugated polymer that in exposure to oxygen and/or moisture results *p*-doped [32–34]. The depletion layer capacitance can be readily recognized by a bias voltage-dependence that follows the Mott-Schottky (MS) characteristics, i.e., linear C^{-2} vs. V. A measurement of the capacitance vs. voltage in the dark shows a straight MS curve over a wide bias-voltage range (inset in Fig. 2(a)). This allows us to calculate the built-in voltage (flat-band conditions at the cathode) V_{bi}=0.35 V and acceptor concentration N_A=1.1 $\times 10^{15}\,\mathrm{cm}^{-3}$, assuming ε=3 for P3HT:PCBM [24]. It should be remarked that the built-in voltage refers to one particular interface and does not set a limit to the photovoltage in the solar cell, which is determined by the separation of Fermi levels and selectivity of contacts [28], as discussed later. At larger reverse bias the organic layer becomes fully depleted because of the thinness of the layer, $L \approx 100$ nm, and the capacitance levels off to the geometric value ($C_g=\varepsilon\varepsilon_0/L$).

Since the bulk active layer is *p*-doped, the V_{oc} at low illumination values is due to the rise of the electron Fermi level, while E_{Fp} remains stationary, see Eq. (1). As E_{Fn} increases, the capacitance is determined by two separate components. They are connected in parallel and both are bias voltage-dependent. The first is the surface-depletion capacitance, as already mentioned, that increases rather slowly. The second is the chemical capacitance, associated with the homogeneous accumulation of charge carriers, with density n, in the photoactive layer [27,35]

$$C_\mu^{(n)} = Lq^2 \frac{dn}{dE_{Fn}} \tag{3}$$

Here the capacitance is given per unit area. It should be observed that the voltage used in the small perturbation measurement is $dV=dE_{Fn}/q$, see Eq. (2).

At increasing E_{Fn} the chemical capacitance increases steeply and overcomes the depletion layer capacitance [15]. Furthermore, using the zero-temperature approximation of the Fermi function at occupancy $>1\%$ [36], the chemical capacitance follows the shape of the electron DOS, g_n, as

$$C_\mu^{(n)} = Lq^2 g_n(E_{Fn}) \tag{4}$$

The capacitance values reported in Fig. 2(a) are well described by the previous model. At $V_{oc} \approx 0$ the capacitance coincides with the geometric value. At low V_{oc} values, the capacitance increases indicating the reduction of the depletion layer thickness. For values in excess of $V_{oc} \approx 0.35$ V, the capacitance reflects the shape of the DOS of electrons. It is important to point out that the capacitance rapidly rises even at the highest V_{oc} values that can be measured. This is in contrast to the results obtained in the dark [24], where a decrease of capacitance is observed at high applied

bias voltage V. These experimental results therefore permit the determination of the DOS in a restricted domain of photovoltages.

It should also be remarked that there is a shift of voltage in C–V characteristics under illumination, with respect to dark conditions, which was attributed to the charging of surface states at the metal/organic interface in the external contact [30].

3.2. The density-of-states in the electron transport material

The description of carrier transport in organic semiconductors usually assumes a wide DOS with a Gaussian shape [37,38]

$$g_n(E-E_L)=\frac{N_n}{\sqrt{2\pi}\sigma_n}\exp\left[-\frac{(E_L-E)^2}{2\sigma_n^2}\right] \quad (5)$$

Here N_n is a total density per unit volume, E_L is the center of the DOS and σ_n the disorder parameter. This type of distribution reflects the energy disorder caused by electrostatic [39] and steric [40] interactions resulting from the different environment in which each molecule is placed. The LUMO manifold then spreads in energy as a result of long-range electrostatic (dipolar) interactions with the surrounding disordered host [37]. This is particularly true for a blend made up of two different, disordered materials. It should be also pointed out that Eq. (5) is a first approximation, and more accurate determinations of the DOS reveal additional characteristics. Hulea et al. showed [41] that the total DOS for poly(p-phenylene vinylene) is well described by means of a more featured structure which includes two Gaussian shapes. In our experiments the higher energy states are not accessible because the recombination kinetics severely limits occupation to the DOS tail, and therefore we maintain the interpretation based on a single Gaussian function as stated in Eq. (5).

A fit of the capacitance values to a Gaussian DOS is presented in Fig. 3. In the following we discuss the representative values of the parameters obtained from the fits of several solar cells. The disorder parameter σ_n, which accounts for the broadening of the Gaussian DOS, lies within the range 125–140 meV, in good agreement with values found in most cases for conducting polymers $\sigma_n \approx 0.1$ eV [42]. In case of pure PCBM devices, values for σ_n=73 meV were reported to interpret mobility dependence on temperature according to disordered hopping transport models [43]. In our direct measurements the disorder parameter is considerably higher, what points to the fact that energetic disorder is enhanced in the blend presumably by additional dipole interactions.

The total electron density results in $N_n=1-2\times10^{18}$ cm^{-3}. This value appears to be very low and predicts an average distance between the centers of PCBM molecules of 8–10 nm. From simple geometric considerations about the volume occupation of PCBM phase (the Van der Walls diameter of the PCBM molecule about 1 nm), the expected total density would be around $N_{PCBM}=10^{20}$ cm^{-3}. The ratio N_n/N_{PCBM} reaches the values within the range 1–2% for different cells. These results may indicate the existence of additional states at higher energies as observed by Hulea et. al [41].

The results from the fits of several cells are centered at E_L=0.75–0.80 eV. Note that this value should be associated with *effective* E_{LUMO} energy for PCBM in the blend, relative to the Fermi level of holes in P3HT, $E_L \approx E_{LUMO}-E_{Fp}$. The energy position of the Gaussian DOS center ($E_L=0.75-0.80$ eV), which corresponds to half occupation of the electron DOS, results smaller than the effective gap between the LUMO level of PCBM and the HOMO of P3HT ($E_g\sim1.1$ eV). This is due to the fact that the DOS of P3HT should be also broad and one may expect $E_g-E_L \approx E_{FP}-E_{HOMO} \approx 0.2$eV. The different energy levels are diagrammatically indicated in Fig. 4. The value $E_L=0.75-0.80$ eV should be viewed as an upper limit of the splitting of the quasi-Fermi levels. It follows that to reach higher V_{oc} values it would be necessary not only blends with a large effective band gap but also to increase the occupation of the DOS manifold. As we will see below the DOS occupation is severely limited by the growth of the recombination rate at high irradiation levels.

Since the doping level is relatively low, we show later that under illumination the hole density exceeds the initial value. It is thus possible to obtain an additional contribution to the measured capacitance from $C_\mu^{(p)}$, the chemical capacitance associated to the HOMO manifold of P3HT, in addition to $C_\mu^{(n)}$. The actual observation of $C_\mu^{(p)}$ depends on the ability to move E_{Fp} as the HOMO occupation progresses. From Eq. (1) we obtain $-qdV_{oc}=dE_{Fn}-dE_{Fp}$, and assuming electroneutrality $n=p$, it is easy to show that the relative displacement of Fermi levels depends on the ratio of the DOS at the Fermi levels:

$$dE_{Fp}=-\frac{C_\mu^{(n)}}{C_\mu^{(p)}}dE_{Fn}=-\frac{g_n(E_{Fn})}{g_p(E_{Fp})}dE_{Fn} \quad (6)$$

As an example, in DSC composed of an organic hole conductor (instead of liquid electrolyte) it is observed that the hole density

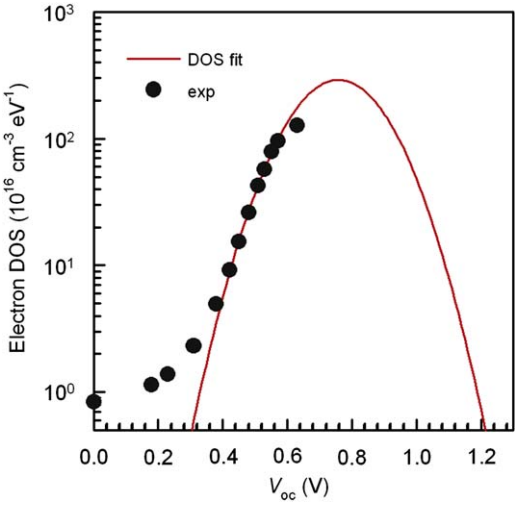

Fig. 3. Calculated electron DOS from the capacitance values exhibiting a Gaussian shape with total density of LUMO levels $N=1.1(0.1)\times10^{18}$ cm^{-3}, center of the DOS $E_0=0.76(0.02)$ eV, and dispersion parameter $\sigma=128(7)$ meV.

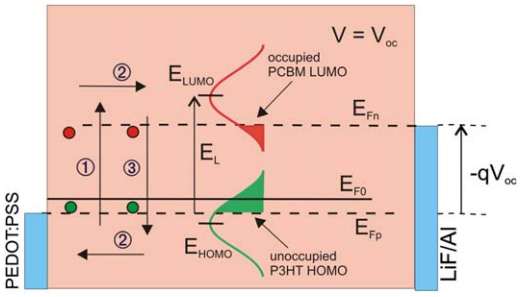

Fig. 4. Band structure of the P3HT:PCBM heterojunction in steady-state illumination under open-circuit conditions ($V=V_{oc}$). Main dynamic processes occurring in the blend layer: excess holes and electrons are photogenerated (1) into the P3HT HOMO and PCBM LUMO manifolds, respectively. Charge carriers diffuse along the diode bulk (2), and eventually recombine (3). Molecular orbitals spread in energy (DOS) following Gaussian shapes. The occupancy level of LUMO (HOMO) states is determined by competing photogeneration and recombination rates. This in turn governs the achievable V_{oc} which depends on the splitting of the quasi-Fermi levels, $-qV_{oc}=E_{Fn}-E_{Fp}$. The DOS centers are located at E_{LUMO} and E_{HOMO}, respectively. The relative position of the Fermi level in the dark E_{F0} is also indicated.

increases at high forward voltage [44], and information on carrier densities can be obtained from a separate determination of electron and hole conductivities. However, in the case of P3HT:PCBM solar cell this is a complex topic that lies beyond the scope of the present work. Later in this work we comment on the implications of a displacement of the Fermi level of both carriers.

3.3. Recombination kinetics

The effective electron lifetime $\tau_n = R_{\rm rec} C_\mu^{(n)}$ can be readily determined from the low-frequency part of the impedance spectra [9,45], which exhibits a *RC* parallel circuit as observed in Fig. 1. Following this procedure we found electron effective lifetime values within the time interval 1–100 μs (for $V_{\rm oc} > 0.4$ V), decreasing as the bias increases, as shown in Fig. 2(c). The steady-state carrier density can be calculated by integration of the capacitance at a given $V_{\rm oc}$ value as

$$n = \frac{1}{qL}\int_0^{V_{\rm oc}} C_\mu{}^{(n)}(V)\,dV \tag{7}$$

We represent in Fig. 5 the lifetime as a function of the charge carrier n calculated from the values in Fig. 2(a). By examining this plot one can distinguish an interval which exhibits a linear relation with the inverse of the carrier density. Longer τ_n values deviate from the linear relation because the capacitance involved is not related to the carrier storage [Eq. (4)] but to the junction capacitance. At high illumination levels ($V_{\rm oc} > 0.6$ V) recombination time results shorter than expected. Experimental exponents in the relation $\tau \propto n^{-\beta}$ always result within the interval $\beta = 0.95 - 1.05$.

Recombination time most likely refers to losses produced by electron-hole bimolecular recombination of free carriers along the absorber layer, although recombination routes at contact surfaces cannot be completely excluded. Under the assumption that bulk recombination mainly determines the loss path for electron-hole pairs, bimolecular recombination rate is given by

$$\frac{dn}{dt} = -\gamma np \tag{8}$$

where n and p correspond to the steady-state electron and hole density, respectively. γ stands for the recombination coefficient. Doping levels extracted from the Mott-Schottky plots in Fig. 1 lie within the range of $p_0 = N_A \approx 10^{15}$ cm^{-3}. As observed in Fig. 5 photogenerated carriers reach values of 10^{17} cm^{-3} at 1 sun illumination ($V_{\rm oc} \approx 0.6$ V). This means that $p > N_A$ and one can assume $n = p$. In order to derive a lifetime from Eq. (8) we apply small perturbation conditions [9,11] and we obtain

$$\frac{d\Delta n}{dt} = -2\gamma n \Delta n, \tag{9}$$

resulting

$$\tau_n = \frac{1}{2\gamma n}. \tag{10}$$

Alternatively, recalling Eq. (2) and taking into account the recombination current density $j_{rec} = L\gamma n^2$ that is obtained from the bimolecular law with $n = p$, one can obtain that $R_{rec}^{-1} = 2\gamma n C_\mu^{(n)}$, and Eq. (10) also follows readily.

The linear relation obtained for the lifetime on charge-carrier density in Fig. 5 then corroborates the bimolecular recombination mechanism assumed in Eq. (8), with a constant recombination coefficient γ uniform within the illumination range used.

From the prefactor in the linear relationship in Fig. 5 one can derive a value for the recombination coefficient [Eq. (8)] which results in $\gamma = 6 \times 10^{-13}$ cm^3 s^{-1}. Our result coincides with values recently obtained from transient photovoltage and absorption signals [23] for P3HT:PCBM blends, although in this last study γ results concentration dependent. In another recent study [46] based on steady-state current–voltage characteristics it was suggested that the slowest carrier (holes) dominates bimolecular recombination coefficient, assuming Langevin mechanism in which $\gamma_L = q(\mu_h + \mu_e)/\varepsilon$. Since for the blend P3HT:PCBM it is widely believed that $\mu_e > \mu_h$ the recombination coefficient would be exclusively related to the slowest carrier as $\gamma_h = q\mu_h/\varepsilon$. However, using characteristic values of hole mobility $\sim 10^{-5} - 10^{-4}$ cm^2 V^{-1} s^{-1} [47], we obtain that the experimentally determined $\gamma < \gamma_h$, by at least two orders of magnitude. Therefore the ability of charge carriers to reach P3HT:PCBM interfaces, as derived from mobility-related Langevin-type forms, seems to play a secondary role in the recombination process. The limiting recombination mechanism in P3HT:PCBM BHJs is mainly determined by specific features of the charge-transfer process at the interface between the acceptor molecules and the donor polymer, as discussed further in the next Section. A similar conclusion was obtained for DSC [48].

If G is the effective photogeneration rate of separate charge carriers, the charge-carrier density reached in steady-state illumination will be $n = 2G\tau_n(n)$. At high illumination, $n \propto G^{1/2}$ and τ_n is so small that the storage of photocarriers cannot progress. We consider that this limiting effect lies behind the points in Fig. 5 which deviate from the linear relationship at $V_{oc} > 0.6$ V. Since the open-circuit photovoltage is governed by the relative occupation of the DOS, we can conclude that $V_{\rm oc}$ is finally determined by bimolecular recombination losses.

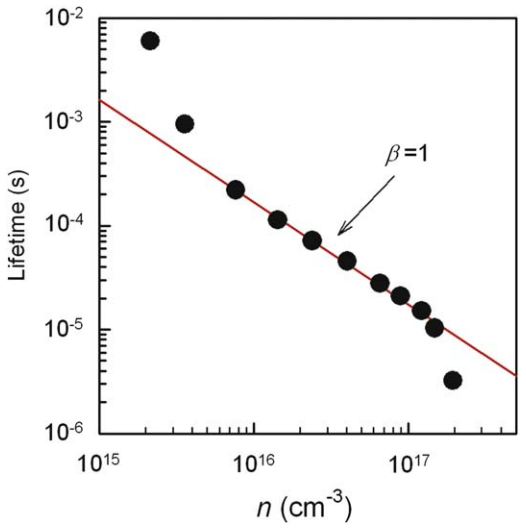

Fig. 5. Recombination time (effective lifetime) as a function of the charge-carrier density, which is obtained by DOS integration. A linear relationship is obtained $\beta = 1$.

3.4. Charge transfer in disorder model

As it has been already discussed, a simple model based on Eq. (8) provides a good description of the measured values of recombination lifetime. However, the interpretation of the lifetime and capacitance using the simple model, opens a number of questions that require further clarification. We next discuss these questions in order to point out the direction for further experimental investigations.

First, the dependence of measured lifetime on carrier density shows that under illumination, there is a displacement of the Fermi level of *both* electron and hole carriers, a question partially commented before. Therefore the lifetime at high irradiation level

cannot be attributed to a specific carrier, and it becomes important to establish a more general model in which the perturbation used to measure impedance (or any transient method) affects both carriers. To solve this question, we present in the Appendix the solution of impedance response of a model that allows to define separately the lifetimes of electrons and holes,

$$\tau_n = r_{rec}^{(n)} c_\mu^{(n)} \tag{11}$$

$$\tau_p = r_{rec}^{(p)} c_\mu^{(p)} \tag{12}$$

where the recombination resistances (r_{rec}) and chemical capacitances (c_μ) are defined in the Appendix. We have also shown in the Appendix that the measured lifetime τ_{eff} relates to those in Eqs. (11) and (12) as

$$\tau_{eff} = \frac{\tau_n \tau_p}{\tau_n + \tau_p} \tag{13}$$

According to Eq. (13), if $\tau_n \ll \tau_p$ then $\tau_{eff} \approx \tau_n$. Therefore the lifetime measured from the frequency at the top of the impedance arc, is that of the carrier with the shorter lifetime.

Another important question that is implied by the experimental results is the need to consider the process of charge transfer between the two components of the BHJ in more detail, taking into account the energy disorder that is clearly revealed by the capacitance data. In the following paragraphs, we outline a reasonable model for dependence of lifetimes of electrons and holes on the Fermi levels of both carriers.

From the picture of the DOS for electrons and holes outlined in Fig. 4, we describe the electron DOS with Eq. (5) and the hole DOS with a similar expression with parameters N_p, E_H and σ_p. We focus on the electron lifetime $\tau_n \ll \tau_p$ defined in Eq. (11), but the hole lifetime can calculated by an obviously similar method. The total carrier density can be obtained from integration of the DOS

$$n = \int g_n(E_L - E_n) F(E_n - E_{Fn})\, dE_n \tag{14}$$

where F is the Fermi-Dirac distribution function

$$F(E - E_{Fn}) = \frac{1}{1 + \exp[(E - E_{Fn})/k_B T]} \tag{15}$$

The chemical capacitance per unit volume is obtained from Eq. (3), by derivation of Eq. (14)

$$c_\mu^{(n)} = \frac{q^2}{k_B T} \int g_n(E_L - E_n) F(E_n - E_{Fn})[1 - F(E_n - E_{Fn})]\, dE_n \tag{16}$$

The essential ingredient of the calculation of the electron lifetime is to formulate a detailed model for the recombination rate, in order to calculate $r_{rec}^{(n)}$ defined in Eq. (A16), considering that electrons in the occupied states of the LUMO distribution at the energy E_n have a probability to recombine with the hole-containing states at the energy E_p in the HOMO distribution. The probability of charge-transfer events at the organic/organic interface, ν_{rec}, is a notoriously difficult subject [49] and we adopt a relatively simple and general approach based on the assumption of the Marcus model (or polaron hopping), involving a reorganization energy λ [50,51]

$$\nu_{rec}(E_n - E_p) = k_0 \exp\left[-\frac{(E_n - E_p - \lambda)^2}{4 k_B T \lambda} \right] \tag{17}$$

where k_0 is a parameter with dimension ($\mathrm{cm^3\ s^{-1}}$). The recombination flux, per unit device area, is given by the expression [52]

$$j_{rec} = qL \iint g_n(E_L - E_n) F(E_n - E_{Fn}) g_p(E_H - E_p) \times [1 - F(E_p - E_{Fp})] \nu_{rec}(E_n - E_p)\, dE_n\, dE_p \tag{18}$$

The recombination resistance $r_{rec}^{(n)}$ is found by derivation of Eq. (18) with respect to E_{Fn}.

$$[r_{rec}^{(n)}]^{-1} = \frac{q}{k_B T} \iint g_n(E_L - E_n) F(E_n - E_{Fn})[1 - F(E_n - E_{Fn})] \times g_p(E_H - E_p)[1 - F(E_p - E_{Fp})] \nu_{rec}(E_n - E_p)\, dE_n\, dE_p \tag{19}$$

Then the electron lifetime can be found by Eq. (11).

A useful approximation that simplifies the preceding expressions, already mentioned before, is to assume that the Fermi level separates occupied and unoccupied states (zero temperature limit of the Fermi-Dirac distribution). Then by an integration by parts Eq. (16) gives Eq. (4). A similar procedure allows to reduce Eq. (19), and the resulting lifetime is

$$\tau_n(E_{Fn}, E_{Fp}) = \frac{k_0}{q} \int g_p(E_H - E_p)\left[1 - F(E_p - E_{Fp})\right] \times \exp\left[-\frac{(E_{Fn} - E_p - \lambda)^2}{4 k_B T \lambda} \right] dE_p \tag{20}$$

Using the same method we can obtain the lifetime of holes

$$\tau_p(E_{Fn}, E_{Fp}) = \frac{k_0}{q} \int g_n(E_L - E_n) F(E_n - E_{Fn}) \times \exp\left[-\frac{(E_n - E_{Fp} - \lambda)^2}{4 k_B T \lambda} \right] dE_n \tag{21}$$

Inspection of Eq. (20) shows an important conclusion. The lifetime of electrons is practically independent of the DOS of electrons, and so τ_n is governed by the DOS of holes and its occupancy, and by the charge-transfer rate.

Simulations of the different quantities in the model, as a function of the Fermi level of electrons, are shown in Fig. 6 for reasonable parameter values according to the experimental results. The main parameter is the recombination rate constant taken $k_0 = 1 \times 10^{-15}\ \mathrm{cm^3\ s^{-1}}$ to match the values of the measured lifetime. We present two kinds of simulations. In the first curve, Fig. 6(d), the hole Fermi level is left stationary, so that the density of holes is constant. This simulation allows us to conclude that the lifetime shows a very weak dependence on E_{Fn}. The minimum seen in Fig. 6(d) is the standard activationless point in the Marcus model when the difference of free energies equals the reorganization energy. The simulations also show that Eq. (20) is an excellent approximation to the exact value of the lifetime, calculated from Eq. (19).

In the second simulation shown in Fig. 6(d), we let the Fermi level of holes shift as the Fermi level of electrons raises, so that the density of holes, increases with increasing E_{Fn}, see Fig. 6(a). This has a very large impact on the electron lifetime, that decreases exponentially, as otherwise would be expected from the model based on Eq. (8) already discussed before.

The factors influencing the dependence of the electron lifetime on electron density, are illustrated in Fig. 7. If the reorganization energy becomes larger, then the minimum is displaced to very high Fermi level and could be unobservable. The lifetime then simply shows power law behavior as discussed in the experimental results.

Provided that λ is high, the exponent in $\tau \propto n^{-\beta}$ depends only on the relative displacement of the Fermi levels. Therefore, the critical question for explaining the lifetime variation is to determine the conditions of charge compensation. At high irradiation level it is natural to assume $n = p$, as we commented before. However, the displacement of Fermi levels depends also on the relative values of the DOS, Eq. (6). In addition, the electrostatic compensation may not be directly related to the number of carriers that participate in charge transfer, e.g. if some regions of

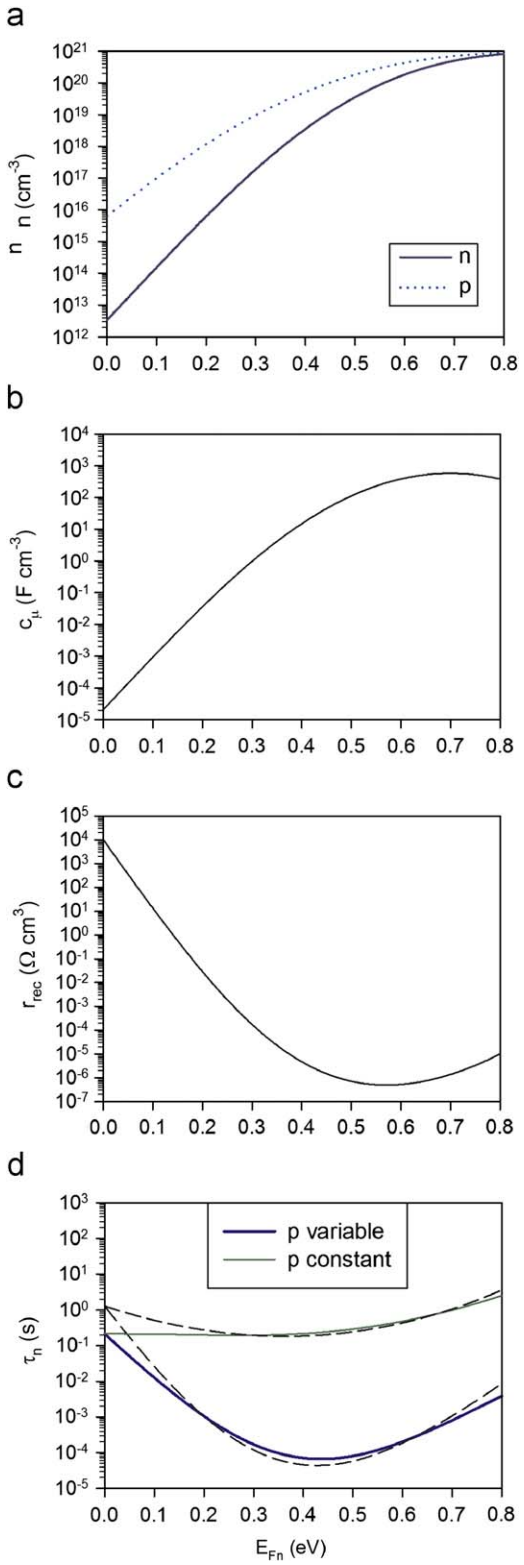

Fig. 6. Calculation of several quantities related to the disorder charge-transfer model, as a function of the electron Fermi level. (a) Electron and hole density. (b) Chemical capacitance of electrons. (c) Recombination resistance. (d) Electron lifetime. It is assumed that the hole Fermi level decreases as $E_{Fp}=-0.8E_{Fn}$. In (d) the lifetime is calculated also for constant $E_{Fp}=0$. The dashed line in (d) is an approximation. Parameters used in the calculation: $N_n=N_p=10^{21}$ cm^{-3}, $E_L=0.7$ eV, $E_H=-0.5$ eV, $\sigma_n=\sigma_p=0.1$ eV, $\lambda=0.5$ eV, $k_0=1\times10^{-15}$ cm^3 s^{-1}.

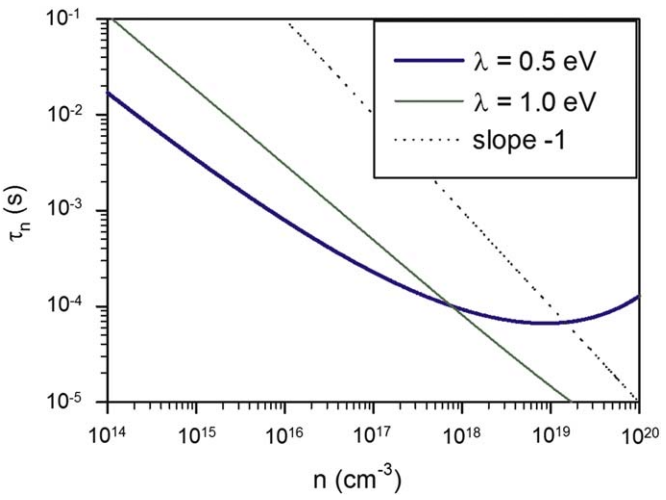

Fig. 7. Calculation of electron lifetime as a function of total electron density in the disorder charge-transfer model, for different values of the reorganization energy as indicated. It is assumed that the hole Fermi level decreases as $E_{Fp}=-0.8E_{Fn}$. Parameters used in the calculation: $N_n=N_p=10^{21}$ cm^{-3}, $E_L=0.7$ eV, $E_H=-0.5$ eV, $\sigma_n=\sigma_p=0.1$ eV, $k_0=1\times10^{-15}$ cm^3 s^{-1}.

the mixed phases become aggregated so that part of the numbers of carriers are isolated. In conclusion, one important question for a more detailed understanding of the carrier lifetime in BHJ is the quantitative determination of the densities of electron and hole carriers, as a function of the photovoltage.

In summary, our results show that the lifetime in BHJ solar cells is very likely dominated by the rate of interfacial charge transfer, which is observed to depend strongly on the relative positions of the electron and hole Fermi levels. We have presented a specific model based on Marcus rates that must be regarded as exploratory, since at this point the set of available data is scarce. We should emphasize that results in another paper [23] are qualitatively similar but indicate a different effective recombination order. More reports on capacitance and lifetime are needed in orden to ascertain the general features of the lifetime in BHJ and how they relate to materials parameters.

4. Conclusion

To conclude, we have shown in this study how impedance spectroscopy is able to reliably determine recombination kinetics and charge–carrier density in organic photovoltaic devices under conditions of continuous irradiation. Recombination rate is enhanced at high illumination levels, and this is viewed as the limiting mechanism for the photogenerated charge accumulation, which finally states the reachable V_{oc} value.

Acknowledgements

We are very grateful to Dr. Martijn Lenes for helpful discussions, Dr. Alejandra Soriano for device preparation and characterization, Dr. Antoni Munar for his collaboration in experimental set-up and Jorge Ferrando for his assistance with the design in the temperature control of the measurement cell. We thank financial support from Ministerio de Ciencia e Innovación under projects HOPE CSD2007-00007, CSD2007-00010, MAT2006-28187-E, Generalitat Valenciana project PROMETEO/2009/058, Universitat Jaume I (P1.1B2008-32), Generalitat Valenciana project

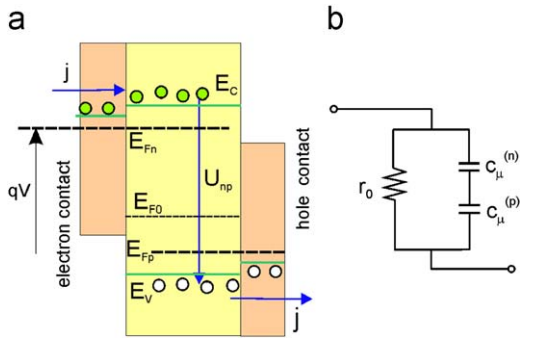

Fig. 8. (a) Basic model of a solar cell consisting on a semiconductor material with selective contacts to electrons and holes. Shown are the Fermi levels for electrons E_{Fn} and holes E_{Fp}, the equilibrium Fermi level E_{F0}, the recombination rate, U_{np}, the transport levels for electrons E_C and holes E_V, the (photo)voltage V, and the electrical current density, j. (b) Equivalent circuit containing the chemical capacitances c_μ and recombination resistances $r_{\rm rec}$ of electrons and holes.

PROMETEO/2009/058, Universitat Jaume I (P1.1B2008-32), and ESF Eurocores-05SONS-FP-021, (MAT2006-28185-E, MAT2006-28187-E).

Appendix

This is a simple model that allows clarifying the meaning of separate lifetimes for electrons, τ_n, and holes, τ_p, with respect to Impedance Spectroscopy measurements, in those systems in which the Fermi levels of both kinds of carriers can be considerably displaced with respect to the equilibrium value. Of course a full model for a solar cell with variation of the concentration of two kinds of carriers, is a complex topic that requires to stipulate a number of aspects: diffusion-drift transport, charge shielding and/or electrical-field distribution via Poisson equation, barriers at the contacts, etc. However, with the mentioned topic in mind we consider only a slab of semiconductor with thickness L, and perfect selective contacts [28], for electrons at $x=0$ and holes at $x=L$, and furthermore we assume that transport is quite fast (i.e., recombination lifetimes are much longer than transit times) for both carriers, so that the carrier densities are nearly homogeneous, see Fig. 8(a). This model [53] is in practice appropriate in conditions close to open-circuit voltage.

We calculate the small-signal ac impedance response of the model of Fig. 8(a), given by

$$Z = -\frac{\hat{\varphi}}{\hat{j}} \tag{A1}$$

where $\hat{\varphi}$ and $\hat{j}$ are the small perturbation voltage and current, respectively. At position x, n is the density of electrons, p is the density of electrons, J_n the flux of electrons and J_p the flux of holes in the positive x direction. The conservation equations are

$$\frac{\partial n}{\partial t} = -\frac{\partial J_n}{\partial x} - U_{np} \tag{A2}$$

$$\frac{\partial p}{\partial t} = -\frac{\partial J_p}{\partial x} - U_{np} \tag{A3}$$

Here, U_{np} is the recombination rate, per unit volume. We do not include carrier photogeneration terms since these not appear in the final ac impedance equations. By integration between 0 and L, Eq. (A2) gives

$$\frac{\partial n}{\partial t} = -\frac{1}{L}[J_n(L) - J_n(0)] - U_{np} \tag{A4}$$

The electrical current at the contacts is given by

$$j = -qJ_n(0) = +qJ_p(L) \tag{A5}$$

and the selectivity conditions imply

$$J_n(L) = J_p(0) = 0 \tag{A6}$$

Therefore from Eqs. (A2) and (A3) we get

$$\frac{\partial n}{\partial t} = -U_{np} - \frac{j}{qL} \tag{A7}$$

$$\frac{\partial p}{\partial t} = -U_{np} - \frac{j}{qL} \tag{A8}$$

The next step is to consider a small harmonic perturbation over a steady state. For example, modulation of the Fermi levels for electron and holes, with small time-dependent voltages $\hat{\varphi}_n$ and $\hat{\varphi}_p$, respectively, can be stated as

$$E_{Fn} = \overline{E}_{Fn} + q\hat{\varphi}_n \tag{A9}$$

$$E_{Fp} = \overline{E}_{Fp} + q\hat{\varphi}_p \tag{A10}$$

Note that the terms with an overbar are constant with time. Expansion of the terms in n, p in Eqs. (A7), (A8), to first order in $\hat{\varphi}$, gives the following results:

$$\frac{\partial n}{\partial t} = \frac{c_\mu^{(n)}}{q}\frac{\partial \hat{\varphi}_n}{\partial t} \tag{A11}$$

$$\frac{\partial p}{\partial t} = \frac{c_\mu^{(p)}}{q}\frac{\partial \hat{\varphi}_p}{\partial t} \tag{A12}$$

Here we have introduced the chemical capacitances per unit volume

$$c_\mu^{(n)} = C_\mu^{(n)}/L \tag{A13}$$

$$c_\mu^{(p)} = C_\mu^{(p)}/L \tag{A14}$$

The expansion of U_{np} leads to

$$\delta U_{np} = \frac{1}{qr_{rec}^{(n)}}\hat{\varphi}_n + \frac{1}{qr_{rec}^{(p)}}\hat{\varphi}_p \tag{A15}$$

where the recombination resistances (per volume) are defined as

$$r_{rec}^{(n)} = ALR_{rec}^{(n)} = \frac{1}{q^2}\left(\frac{\partial U_{np}}{\partial E_{Fn}}\right)^{-1} \tag{A16}$$

$$r_{rec}^{(p)} = ALR_{rec}^{(p)} = \frac{1}{q^2}\left(\frac{\partial U_{np}}{\partial E_{Fp}}\right)^{-1} \tag{A17}$$

We apply in Eqs. (A7) and (A8) the Laplace transform $\partial/\partial t \to i\omega$, where ω is the angular frequency of the perturbation, and we introduce the expansions to first order in $\hat{\varphi} = \hat{\varphi}_n + \hat{\varphi}_p$. We obtain the set of linear equations

$$\left(i\omega c_\mu^{(n)} + \frac{1}{r_{rec}^{(n)}}\right)\hat{\varphi}_n + \frac{1}{r_{rec}^{(p)}}\hat{\varphi}_p = -\frac{\hat{j}}{L} \tag{A18}$$

$$\frac{1}{r_{rec}^{(n)}}\hat{\varphi}_n + \left(i\omega c_\mu^{(p)} + \frac{1}{r_{rec}^{(p)}}\right)\hat{\varphi}_p = -\frac{\hat{j}}{L} \tag{A19}$$

Solving these equations, we arrive at the expression of the impedance

$$Z = \frac{1}{L}\frac{c_\mu^{(n)} + c_\mu^{(p)}}{c_\mu^{(n)}/r_{rec}^{(p)} + c_\mu^{(p)}/r_{rec}^{(n)} + i\omega c_\mu^{(n)} c_\mu^{(p)}} \tag{A20}$$

Then Eq. (A20) can be written in a more convenient form

$$Z = \frac{1}{L}\frac{r_0}{1 + i\omega\tau_{eff}} \tag{A21}$$

where τ_{eff} is related to the lifetimes of electrons and holes as indicated in Eq. (13) and

$$r_0 = \frac{(c_\mu^{(n)} + c_\mu^{(p)}) r_{rec}^{(n)} r_{rec}^{(p)}}{\tau_n + \tau_p} \tag{A22}$$

Eq. (A21) shows that the impedance is a parallel *RC* circuit, as indicated in Fig. 8(b), with the resistance r_0. The impedance spectrum of this model is a single arc with a characteristic frequency $\omega_{rec} = \tau_{eff}^{-1}$. The capacitance of the circuit is deduced from

$$c_{eff} = \frac{\tau_{eff}}{r_0} = \frac{c_\mu^{(n)} c_\mu^{(p)}}{c_\mu^{(n)} + c_\mu^{(p)}} \tag{A23}$$

Therefore, the chemical capacitances of electrons and holes are connected in series, which entails that c_{eff} will be determined by the smaller capacitance. The measured capacitance slightly underestimates the actual $c_\mu^{(n)}$ value.

References

[1] C.J. Brabec, N.S. Sariciftci, C. Hummelen, Plastic Solar Cells, Advanced Materials 11 (2001) 15–26.

[2] S.H. Park, A. Roy, S. Beaupré, S. Cho, N. Coates, J.S. Moon, D. Moses, M. Leclerc, K. Lee, A.J. Heeger, Bulk heterojunction solar cells with internal quantum efficiency approaching 100%, Nature Photonics 3 (2009) 297–302.

[3] F.C. Krebs, S.A. Gevorgyan, J. Alstrup, A roll-to-roll process to flexible polymer solar cells: model studies, manufacture and operational stability studies, Journal of Materials Chemistry 19 (2009) 5442–5451.

[4] F.C. Krebs, et al., A round robin study of flexible large-area roll-to-roll processed polymer solar cell modules, Solar Energy Material and Solar Cells 93 (2009) 1968–1977.

[5] W. Ma, C. Yang, X. Gong, K.-S. Lee, A.J. Heeger, Thermally stable, efficient polymer solar cells with nanoscale control of the interprenetating network morphology, Advanced Functional Materials 15 (2005) 1617–1622.

[6] C.J. Brabec, A. Cravino, D. Meissner, N.S. Sariciftci, T. Fromherz, M.T. Rispens, L. Sanchez, J.C. Hummelen, Origin of the Open Circuit Voltage of Plastic Solar Cells, Advanced Materials 11 (2001) 374–380.

[7] L.J.A. Koster, V.D. Mihailetchi, R. Ramaker, P.W.M. Blom, Light intensity dependence of open-circuit voltage of polymer:fullerene solar cells, Applied Physics Letters 86 (2005) 123509.

[8] Q. Wang, S. Ito, M. Grätzel, F. Fabregat-Santiago, I. Mora-Seró, J. Bisquert, T. Bessho, H. Imai, Characteristics of High Efficiency Dye-sensitized Solar Cells, Journal of Physical Chemistry B 110 (2006) 19406–19411.

[9] J. Bisquert, F. Fabregat-Santiago, I. Mora-Seró, G. Garcia-Belmonte, S. Giménez, Electron Lifetime in Dye-Sensitized Solar Cells: Theory and Interpretation of Measurements, Journal of Physical Chemistry C 113 (2009) 17278–17290.

[10] F. Fabregat-Santiago, J. Bisquert, E. Palomares, L. Otero, D. Kuang, S.M. Zakeeruddin, M. Grätzel, Correlation between Photovoltaic Performance and Impedance Spectroscopy of Dye-Sensitized Solar Cells Based on Ionic Liquids, Journal of Physical Chemistry C 111 (2007) 6550–6560.

[11] A. Zaban, M. Greenshtein, J. Bisquert, Determination of the electron lifetime in nanocrystalline dye solar cells by open-circuit voltage decay measurements, Chem Phys Chem 4 (2003) 859–864.

[12] K. Miettunen, J. Halme, P. Lund, Segmented Cell Design for Improved Factoring of Aging Effects in Dye Solar Cells, The Journal of Physical Chemistry C 113 (2009) 10297–10302.

[13] R.A. Sinton, A. Cuevas, Contactless determination of current–voltage characteristics and minority-carrier lifetimes in semiconductors from quasi-steady-state photoconductance data, Applied Physics Letters 69 (1996) 2510–2512.

[14] I. Mora-Seró, Y. Luo, G. Garcia-Belmonte, J. Bisquert, D. Muñoz, C. Voz, J. Puigdollers, R. Alcubilla, Recombination rates in heterojunction silicon colar cells analyzed by impedance spectroscopy at forward bias and under illumination, Solar Energy Materials and Solar Cells 92 (2008) 505–509.

[15] I. Mora-Seró, G. Garcia-Belmonte, P.P. Boix, M.A. Vázquez, J. Bisquert, Impedance characterisation of highly efficient silicon solar cell under different light illumination intensities, Energy & Environmental Science 2 (2009) 678–686.

[16] A. Pivrikas, N.S. Sariciftci, G. Juska, R. Österbacka, A review of charge transport and recombination in polymer/fullerene organic solar cells, Progress in Photovoltaics: Research and Applications 15 (2007) 677–696.

[17] C. Arndt, U. Zhokhavets, M. Mohr, G. Gobsch, M. Al-Ibrahim, S. Sensfuss, Determination of polaron lifetime and mobility polymer/fullerene solar cells by means of photoinduced absorption, Synthetic Metals 147 (2004) 257–260.

[18] C.G. Shuttle, B. O'Regan, A.M. Ballantyne, J. Nelson, D.D.C. Bradley, J.R. Durrant, Bimolecular recombination losses in polythiophene:Fullerene solar cells, Physical Review B 78 (2008) 113201.

[19] A.J. Mozer, G. Dennler, N.S. Sariciftci, M. Westerling, A. Pivrikas, R. Österbacka, G. Juska, Time-dependent mobility and recombination of the photoinduced charge carriers in conjugated polymer/fullerene bulk heterojunction solar cells, Physical Review B 72 (2005) 035217.

[20] G. Dennler, A.J. Mozer, G. Juska, A. Pivrikas, R. Österbacka, A. Fuchsbauer, N.S. Sariciftci, Charge carrier mobility and lifetime versus composition of congugated polymer/fullerene bulk-heterojunction solar cells, Organic Electronics 7 (2006) 229–234.

[21] G. Juska, G. Sliauzys, K. Genevicius, K. Arlauskas, A. Pivrikas, M. Scharber, G. Dennler, N.S. Sariciftci, R. Österbacka, Charge-carrier transport and recombination in thin insulating films studied via extraction of injected plasma, Physical Review B 74 (2006) 115314.

[22] A. Pivrikas, G. Juska, A.J. Mozer, M. Scharber, K. Arlauskas, N.S. Sariciftci, H. Stubb, R. Österbacka, Bimolecular recombination coefficient as a sensitive testing parameter for low-mobility solar-cell materials, Physical Review Letters 94 (2005) 176806.

[23] C.G. Shuttle, B. O'Regan, A.M. Ballantyne, J. Nelson, D.D.C. Bradley, J. de Mello, J.R. Durrant, Experimental determination of the rate law for charge carrier decay in a polythiophene:Fullerene solar cell, Applied Physics Letters 92 (2008) 093311.

[24] G. Garcia-Belmonte, A. Munar, E.M. Barea, J. Bisquert, I. Ugarte, R. Pacios, Charge carrier mobility and lifetime of organic bulk heterojunctions analyzed by impedance spectroscopy, Organic Electronics 9 (2008) 847–851.

[25] J. Bisquert, Chemical capacitance of nanostructured semiconductors: its origin and significance for heterogeneous solar cells, Physical Chemistry Chemical Physics 5 (2003) 5360–5364.

[26] J. García-Cañadas, F. Fabregat-Santiago, H.J. Bolink, E. Palomares, G. Garcia-Belmonte, J. Bisquert, Synthetic Metals 156 (2006) 944.

[27] J. Bisquert, F. Fabregat-Santiago, I. Mora-Seró, G. Garcia-Belmonte, E.M. Berzosa, E. Palomares, A review of recent results on electrochemical determination of the density of electronic states of nanostructured metal-oxide semiconductors and organic hole conductors, Inorganica Chimica Acta 361 (2008) 684–698.

[28] J. Bisquert, D. Cahen, S. Rühle, G. Hodes, A. Zaban, Physical chemical principles of photovoltaic conversion with nanoparticulate, mesoporous dye-sensitized solar cells, Journal of Physical Chemistry B 108 (2004) 8106–8118.

[29] M. Scharber, D. Mühlbacher, M. Koppe, P. Denk, C. Waldauf, A.J. Heeger, C.J. Brabec, Design rules for donor bulk-heterojunction solar cells-Towards 10% energy-conversion efficiency, Advanced Materials 18 (2006) 789–794.

[30] J. Bisquert, G. Garcia-Belmonte, A. Munar, M. Sessolo, A. Soriano, H.J. Bolink, Band unpinning and photovoltaic model for P3HT-PCBM organic bulk heterojunctions under illumination, Chemical Physics Letters 465 (2008) 57–62.

[31] G. Dennler, C. Lungenschmied, N.S. Saricifti, R. Schwödiauer, S. Bauer, H. Reiss, Unusual electromechanical effects in organic semiconductor Schottky contacts: between piezoelectricity and electrostriction, Applied Physics Letters 87 (2005) 163501.

[32] M.S.A. Abdou, F.P. Orfino, Y. Son, S. Holdcroft, Interaction of Oxygen with Conjugated Polymers: Charge Transfer Complex Formation with Poly(3-alkylthiophenes), Journal of American Chemical Society 119 (1997) 4518–4524.

[33] S. Hoshino, M. Yoshida, S. Uemura, T. Kodzasa, N. Takada, T. Kamata, K. Yase, Influence of moisture on device characteristics of polythiophene-based field-effect transistors, Journal of Applied Physics 95 (2004) 5088–5093.

[34] E.J. Meijer, A.V.G. Mangnus, C.L. Huisman, G.W. t'Hooft, D.M. de Leeuw, T.M. Klapwijk, Photoimpedance spectroscopy of poly(3-hexyl thiophene) metal–insulator–semiconductor diodes, Synthetic Metals 142 (2004) 53–56.

[35] J. Bisquert, Chemical capacitance of nanostructured semiconductors: its origin and significance for heterogeneous solar cells, Physical Chemistry Chemical Physics 5 (2003) 5360–5364.

[36] Z. Pomerantz, A. Zaban, S. Ghosh, J.-P. Lellche, G. Garcia-Belmonte, J. Bisquert, Capacitance, spectroelectrochemistry and conductivity of polarons and bipolarons in a polydicarbazole based conducting polymer, Journal of Electroanalytical Chemistry 614 (2008) 49–60.

[37] H. Bässler, Charge transport in disordered organic photoconductors, Physical Status Solid (b) 175 (1993) 15–56.

[38] J. Bisquert, Interpretation of electron diffusion coefficient in organic and inorganic semiconductors with broad distributions of states, Physical Chemistry Chemical Physics 10 (2008) 3175–3194.

[39] S.V. Novikov, D.H. Dunlap, Kenkre, Parris and Vannikov, Essential role of correlations in governing charge transport in disordered organic materials, Physical Review Letters 81 (1998) 4472–4476.

[40] Z.G. Yu, D.L. Smith, A. Saxena, R.L. Martin, A.R. Bishop, Molecular geometry fluctuation model for the mobility of conjugated polymers, Physical Review Letters 84 (2000) 721–724.

[41] I.N. Hulea, H.B. Brom, A.J. Houtepen, D. Vanmaekelbergh, J.J. Kelly, E.A. Meulenkamp, Wide energy-window view on the density of states and hole mobility in poly(p-phenylene vinylene), Physical Review Letters 93 (2004) 166601.

[42] J. Bisquert, G. Garcia-Belmonte, J. García-Cañadas, Effect of the Gaussian energy dispersion on the statistics of polarons and bipolarons in conducting polymers, Journal of Chemical Physics 120 (2004) 6726–6733.

[43] V.D. Mihailetchi, J.K.J. van Duren, P.W.M. Blom, J.C. Hummelen, R.A.J. Janssen, J.M. Kroon, M.T. Rispens, W.J.H. Verhees, M.M. Wienk, Electron transport in a methanofullerene, Advanced Functional Material 13 (2003) 43–46.

[44] F. Fabregat-Santiago, E.M. Barea, J. Bisquert, G.K. Mor, K. Shankar, C.A. Grimes, High carrier density and capacitance in TiO2 nanotube arrays induced by electrochemical doping, Journal of American Chemical Society 130 (2008) 11312–11316.

[45] J. Bisquert, Theory of the Impedance of Electron Diffusion and Recombination in a Thin Layer, Journal of Physical Chemistry B 106 (2002) 325–333.
[46] L.J.A. Koster, V.D. Mihailetchi, P.W.M. Blom, Bimolecular recombination in polymer/fullerene bulk heterojunction solar cells, Applied Physics Letters 88 (2006) 052104.
[47] C. Tanase, E.J. Meijer, P.W.M. Blom, D.M. de Leeuw, Unification of the hole transport in polymeric field effect-transistors and LED, Physical Review Letters 91 (2003) 216601.
[48] J. Bisquert, Chemical diffusion coefficient in nanostructured semiconductor electrodes and dye-sensitized solar cells, Journal of Physical Chemistry B 108 (2004) 2323–2332.
[49] V. Arkhipov, P. Heremans, H. Bässler, Why is exciton dissociation so efficient at the interface between a conjugated polymer and an electron acceptor? Applied Physics Letters 82 (2003) 4605–4607.
[50] M.A. Baldo, S.R. Forrest, Interface-limited injection in amorphous organic semiconductors, Physical Review B 64 (2001) 085201.
[51] I.I. Fishchuk, V.I. Arkhipov, A. Kadashchuk, P. Heremans, H. Bässler, Analytic model of hopping mobility at large charge carrier concentration in disordered organic semiconductors: Polarons versus bare charge carriers, Physical Review B 76 (2007) 045210.
[52] J. Bisquert, E. Palomares, C.A. Qiñones, Effect of Energy Disorder in the Interfacial Kinetics of Dye-Sensitized Solar Cells with Organic Hole Transport Material, Journal of Physical Chemistry B 110 (2006) 11284–11290.
[53] J. Bisquert, Beyond the quasi-static approximation: Impedance and capacitance of an exponential distribution of traps, Physical Review B 77 (2008) 235203.